applied optics

Better three-dimensional inspection with structured illumination: speed

Zheng Yang, Alexander Bielke, and Gerd Häusler*

Institute of Optics, Information and Photonics, Friedrich-Alexander-University Erlangen-Nuremberg, Staudtstrasse 7/B2, 91058 Erlangen, Germany
**Corresponding author: Gerd. Haeusler@fau.de*

Received 14 October 2015; revised 21 January 2016; accepted 22 January 2016; posted 22 January 2016 (Doc. ID 252005); published 1 March 2016

Three-dimensional (3D) inspection in the factory requires precision and speed. While customers can select from a wide spectrum of high-precision sensors, the real challenge today is "speed." We discuss the speed of 3D sensors in a general context to provide an understanding of why high-resolution 3D sensors deliver significantly fewer 3D points per second than the available camera pixel rates suggest. The major cause of low speed is the large number E of required exposures due to the unavoidable depth scanning. Through the example of structured-illumination microscopy (SIM), we demonstrate how E can be minimized without reducing precision. We further demonstrate a lateral scanning strategy that operates at a significantly higher speed for macroscopic measurements by avoiding explicit depth scanning. This paper is a follow up on an earlier paper about the precision limits of SIM and exploits the earlier results.

OCIS codes: (120.3930) Metrological instrumentation; (120.3940) Metrology; (120.4630) Optical inspection; (100.2000) Digital image processing.

http://dx.doi.org/10.1364/AO.55.001713

1. INTRODUCTION

Optical three-dimensional (3D) inspection in the factory requires precision and speed. The challenge is not just precision (there are many high-precision sensors on the market), it is the combination of precision and speed. In this paper, we discuss the concept of "speed" and why the acquisition of 3D data requires much more time than does the acquisition of two-dimensional (2D) data, and we identify the places where time is wasted. A major bottleneck is depth scanning. We therefore suggest a modification of structured illumination microscopy (SIM) that exploits the available camera space-bandwidth-speed product (SBSP) more efficiently in order to make 3D metrology as fast as possible. In an earlier paper [1], we developed a physical model of SIM and concluded that SIM is a strong competitor in the race for fast sensors. In [1], the limits of precision are discussed, whereas in the present paper, the emphasis is placed on "speed." Further, we demonstrate a novel concept for fast depth scanning. A modification of this concept avoids explicit depth scanning completely by incorporating it into a lateral object scan.

In the factory, sensors are never fast enough. As a paradigm, we suggest the inspection of semiconductor packaging, where optical 3D sensors are integrated to monitor the co-planarity of solder bumps. As the components commonly display both rough and smooth surface characteristics, 3D sensors should be able to measure both surface types. The solder bumps become smaller and smaller (now ~100 μm), while the required area inspection speed S^A becomes larger (now ~40 $\mathrm{cm}^2/\mathrm{sec}$ with lateral resolution $\delta x \delta y = 25\ \mu\mathrm{m}^2$). Besides the necessary (depth) precision in the micrometer regime, microscopic lateral resolution is required. The required "speed" S^{3D} (SBSP) is in the range of 10^8 3D points/sec.

2. STRUCTURED ILLUMINATION MICROSCOPY AND PRECISION

We first briefly sketch basic aspects of SIM for industrial inspection and summarize the results given in [1].

As illustrated in Fig. 1, SIM is an active focus variation method. A pattern (commonly a sinusoidal fringe) generated by a spatial light modulator (SLM) is projected onto the object surface through a microscope objective. The illuminated surface is imaged by the same objective onto an image detector (a CCD chip), which is at the conjugate image plane of the aerial pattern image. While the object is scanned in depth, the local fringe contrast $C(x, y, z)$ is measured via phase shifting. From the maximum of the contrast curve $C(z)$ at z_0, the surface shape $z_0(x, y)$ can be found.

For the demanded specifications of the SIM, the major parameters of the sensor have to be adjusted carefully. Fringe frequency, aperture, number of phase shifts, and the number

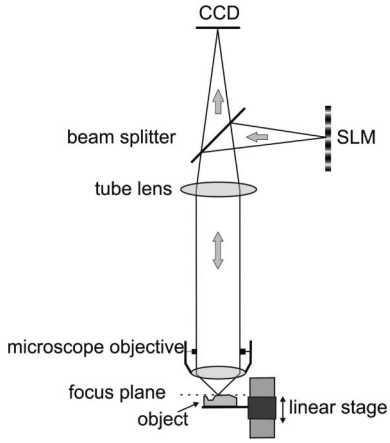

Fig. 1. Working principle of SIM.

of depth scanning steps control the precision and resolution. In [1], a physical model of the signal formation was developed. The model allows for the estimation of the fundamental limit of the precision and its dependence on the system parameters. By means of this model, it is possible to optimize SIM for the greatest precision or for the highest speed. Assuming that an NA 0.85 diffraction-limited lens is used in combination with three sampling points within the half-width of contrast curve, four-phase shift, and a signal-to-noise ratio $\mathrm{SNR}_{\mathrm{shot}} = 100$, a precision of 5 nm and a diffraction-limited lateral resolution can be achieved at its optimal fringe frequency.

To determine the sensor parameters needed for the desired precision, it is important to distinguish between smooth and rough surfaces. On specular surfaces, photon noise limits the precision. An optimal fringe frequency of one-quarter of the cut-off frequency of the modulation transfer function (MTF) for a diffraction-limited optical system will deliver the greatest precision at a diffraction-limited objective. This greatest precision can be further improved by increasing the objective aperture, the number of phase shifts, and the number of depth scanning steps. On rough surfaces, speckle dominates, and the precision is determined primarily by the speckle contrast and Rayleigh depth, as noted by Dorsch *et al.*, for triangulation metrology [2].

For each surface type, there is a fringe frequency-dependent precision function that varies slowly about the optimal frequency. A lower fringe frequency can yield a larger distance of depth scan (resulting from broader contrast curve), allowing for a higher scanning speed. Hence, one can adapt the speed by adjusting the fringe frequency within a wide range without sacrificing too much precision.

3. SPEED BOTTLENECKS

As discussed in [1], the "space-bandwidth-speed product" S^{3D} is a useful parameter for a rough estimate of the speed of a 3D sensor. S^{3D} gives the number of measured 3D points per second. Industries are commonly concerned with the 2D area that is measured per second, the "area inspection speed" $S^{A}(\mathrm{cm}^2/\mathrm{sec})$. Because these parameters depend on the lateral resolution, the precision, and the measurement range, we use a more general speed definition exploiting the sensor channel capacity C^{3D} [3]. A sensor should have a channel capacity not smaller than the limit below:

$$C^{3D} > S^{3D} \log_2\left(1 + \frac{\Delta z_o}{\delta z}\right)[\mathrm{bit}/\mathrm{sec}]. \quad (1)$$

This term includes the space-bandwidth-speed product S^{3D} and the dynamic depth range given by the ratio of the measuring range Δz_o and the precision δz. We also introduce the camera speed S^{2D}, which gives the number of pixels captured per second. We are now ready to compare different sensor concepts and to identify speed bottlenecks. We will always use the example of solder bump inspection, which is a highly challenging and not yet satisfactorily solved task. The required specifications are given in Table 1.

These specifications lead to a required SBSP of $S^{3D} = 160$ million 3D points/sec. At first glance, this requirement should not impose a great challenge, since the fastest available cameras provide $S^{2D} \sim 500\ ^{2D}\mathrm{Mpix}/\mathrm{sec}$. However, 3D data cannot be decoded from just one 2D exposure: because the 2D data encodes three unknowns (the local reflectivity of the surface, the ambient illumination, and the distance), we need at least three independent data for each pixel [4]. There are methods [5,6,7] that try to virtually avoid the unfavorable consequences. However, these sensors display lower precision, lower data density, or lower lateral resolution [8,9]. The paradigm sensor for high speed and precision thus remains the well-known "phase measuring triangulation (PMT)" [10]. PMT requires only $E = 3$ exposures to decipher the three unknowns. For better precision and uniqueness, commonly eight or more exposures are taken. Note that the number of exposures E provides an estimate of the efficiency η of a sensor through $\eta \sim 1/E$.

Scanning white light interferometry (WLI) [11] is extremely precise, but requires a large number of exposures per depth, since the temporal coherence function has to be scanned with sub-micron steps. For our solder bump example, E will be in the range of 5000. If we employ some strong undersampling tricks [12], we can improve the scanning efficiency by factor of 10. With the assumed camera speed $S^{2D} = 500\ ^{2D}\mathrm{Mpix}/\mathrm{sec}$, we achieve $S^{3D} \sim 1.0\ ^{3D}\mathrm{Mpix}/\mathrm{sec}$, which is far less than what is demanded in Table 1.

SIM and confocal microscopy (CM) exploit the contrast/intensity variation versus defocusing, which is not modulated by a carrier. Both methods are more efficient than WLI and require fewer exposures. We estimate $E \sim 100$ for SIM (to be explained below), thus providing $S^{3D} \sim 5.0\ ^{3D}\mathrm{Mpix}/\mathrm{sec}$, which is still far from the required speed. CM delivers roughly the same speed.

Table 1. Table of Specifications for Solder Bump Inspection

Precision δz	<1 μm
Depth measuring range Δz_o	~500 μm
Dynamic range $\log_2(\Delta z_o/\delta z)$	9 bit
Lateral resolution $\delta x, \delta y$	$\delta x \delta y = 25\ \mu\mathrm{m}^2$
Area speed S^A	$\sim 40\ \mathrm{cm}^2/\mathrm{sec}$
S^{3D}	$160\ ^{3D}\mathrm{Mpix}/\mathrm{sec}$
C^{3D}	1.4 Gbit/sec
Surface type	smooth and rough

Since in principle, PMT requires only $E = 3$, why do we need so many exposures? The simple answer is that PMT is commonly used for applications on a macroscopic scale. For "macroscopic" samples, such as car bodies, the measuring range Δz_o is smaller than the Rayleigh depth of focus $\Delta z_R = \delta x^2/\lambda$ of the illumination and the observation.

Because the required lateral resolution δx and Δz_R are coupled, we encounter no problems so long as the object depth satisfies the condition $\Delta z_o < \delta x^2/\lambda$, which is commonly the case for sufficiently large $\delta x (\gg \lambda)$. Indeed, for "macroscopic" applications, PMT is the sensor of choice and would even satisfy the speed requirements of the table above.

For the solder bump inspection, however, the measuring range is larger than the Rayleigh depth of focus: with $\delta x \sim 5\ \mu\text{m}$ and an object depth $\Delta z_o \sim 500\ \mu\text{m}$, we get the ratio $R = \Delta z_o/\Delta z_R = \Delta z_o \lambda/\delta x^2 \sim 10$. This necessarily requires depth scanning. How many depth steps, or exposures E, will be necessary? The ratio R gives only a rough estimate of E. Considering the boundary effects and the number P of phase shifts to evaluate the contrast in the SIM images, we need at least

$$E > \left(\frac{2\Delta z_o \lambda}{\delta x^2} + 3\right) P \qquad (2)$$

exposures [1]. For our application described in Table 1, and with $P = 4$, we need $E = 92$ exposures. This example should clarify why 3D sensors (not only SIM) with microscopic resolutions are slow. The factor 2 in Eq. (2) means that we must sample the contrast function with a sampling distance of at least half the FWHM width ($\sim$½Δz_R). The number "3" stems from boundary effects: for a scan range Δz_o, the number of exposures $E = 2\Delta z_o/\Delta z_R + 1$ seems to be sufficient to cover the entire depth range. However, the depth range has to be extended by another FWHM width to generate a complete signal for the last sampling point at the edge, which leads to two more exposures.

Is it hopeless to make the sensor faster? Equation (2) teaches us that E goes with $1/\delta x^2$. So the first lesson is to design the required demands, specifically the lateral resolution, very carefully. Reducing the lateral resolution improves the efficiency with the square of δx. As the number of necessary pixels per area will be reduced as well, the area speed S^A will remarkably increase with δx^4: 50% less lateral resolution means $\sim$16 times faster measurement.

The second lesson: Eq. (2) includes a factor P that increases the number E significantly. In principle, P has to be greater than or equal to 3 (3 unknowns). Commonly, $P = 4$ is chosen to reduce the influence of nonlinearities. $P > 1$ costs time (exposures), but this is not the major bottleneck: $P > 1$ requires stop-and-go depth scanning, which is technologically unfavorable and time consuming. In the following sections, we explain how to eliminate the stop-and-go and further reduce the number of exposures.

4. EFFICIENT DEPTH SCANNING WITHOUT STOP-AND-GO

As mentioned, the contrast of the observed fringe pattern is not directly measurable. It is calculated from (at least) three phase-shifted intensity images taken at each depth position. The inevitable stop-and-go gives rise to an extremely low speed and to mechanical wear. Several solutions introduced in [13,14,15] try to bypass this problem by exploiting the spatial information. These papers describe how the "local" contrast is extracted via the numeric lateral differentiation of the observed pattern. Due to its noise-amplifying transfer function $\sim\nu$, the differentiation decreases the SNR of the depth signal compared to the phase-shifting method. Another drawback of these solutions is the reduced efficiency η: to calculate one 3D point, the solutions of [13,14,15] all require more exposures than required by the conventional phase-shifting method.

To keep the paper concise, we exemplarily give a qualitative explanation for the efficiency of the method described in [13]; the explanation for [14,15] can be derived in a similar way. In the best scenario, where a planar object is measured by three-phase shifting, at least $E = 9$ exposures are necessary for distance evaluation (three exposures at three depth steps). The solution of [13] uses multiple binary lines instead of a sinusoidal pattern. During the depth scan, the sparse line pattern is laterally moved across the field of view. A contrast curve can be obtained via slope calculation at the line edges. To our knowledge, the smallest line distance implemented in commercial systems is four pixels. So at least $E = 4 \times 3 = 12$ exposures have to be taken within the FWHM of the contrast curve to ensure that each detector pixel can acquire three contrast values, while the line pattern is continuously sliding over the three-pixel gap. The solutions in [14,15] require at least $E = 12$ exposures as well.

To overcome the stop-and-go problem efficiently, we have introduced a novel depth scanning strategy called "flying phase shifting" [16,17], which requires only $E = 5$ exposures. Through this strategy, it is sufficient to acquire only one camera image at each depth position, so the object can be measured with a continuous depth scan. The information efficiency is optimized to its theoretically lower limit, as explained below.

The idea to avoid the stop-and-go originates from amplitude modulation (AM) modulation and was originally reported in [18] for extending the depth of focus of a PMT sensor, where the focus signal is encoded in the envelope of a periodic carrier.

We adapt this concept to SIM by laterally shifting the projected sinusoidal fringes while the object is simultaneously moving (scanned) along the longitudinal direction. The camera takes exposures with a time interval synchronized with the depth scan and the lateral fringe shift. Only one single image is acquired at each depth position. Through the application of this method, the contrast curve $C(z)$ is intrinsically modulated within the envelope of the intensity signal. The measured intensity at each pixel is AM modulated, as expressed in Eq. (3) and illustrated in Fig. 2, and is

$$I(z) = I_0 + I_0 C \cos\left(\frac{2\pi(z - z_0)}{\Delta s P} + \phi_0\right), \qquad (3)$$

where the frequency of the carrier signal is freely tunable through the adjustment of the longitudinal sampling distance Δs and the number of phase shifts P.

By precisely tuning the synchronization between the camera acquisition and the fringe shift, we can explicitly adjust the number P of phase shifts. The case $P = 4$ is illustrated in Fig. 2. Instead of performing phase shifts at fixed z-positions,

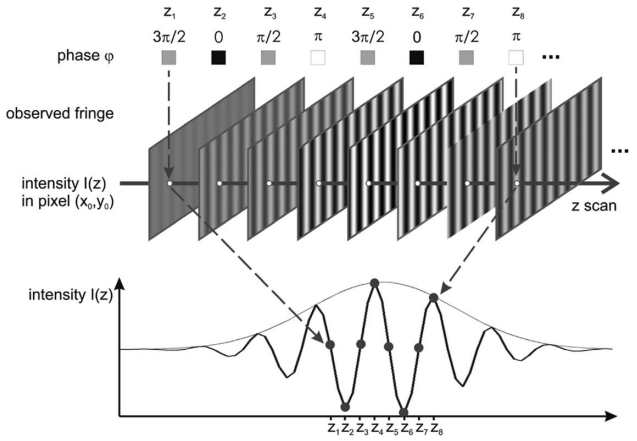

Fig. 2. Continuous depth scan with "flying phase shift."

the fringe pattern is measured only once at each depth position z_1, z_2, z_3, z_4 etc., where the fringes are shifted by 0, $1/2\pi$, π, $3/2\pi$, etc.

The signal $I(z)$ is analogous to the correlogram in white light interferometry, and the envelope can be decoded by well-established methods. There are different implementations, such as filtering in the Fourier domain [19], the Hilbert transformation [20], and other methods [21], but all these methods use essentially the same principle, which is visualized in Fig. 3.

This figure displays a numerically simulated AM signal where the phase at each sampling point is subsequently shifted by 90° steps. The magnitude of its Fourier transform, shown in Fig. 3(b), consists of a delta peak at zero frequency and the convolution of the Fourier spectra of the envelope and carrier signal. After single-sideband demodulation, shown in Fig. 3(b),

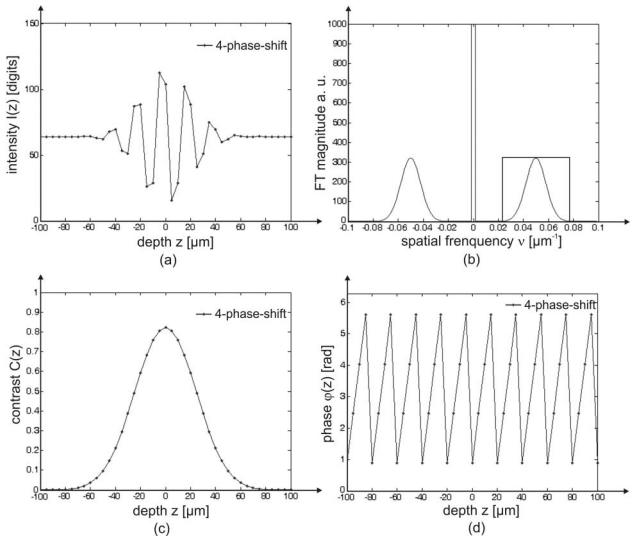

Fig. 3. (a) Simulated AM modulated intensity signal with $P = 4$. (b) Magnitude of Fourier transform of signal in (a) and single-sideband filter. (c) The reconstructed contrast curve calculated from the inverse Fourier transformation of the filtered signal in (b) using the rectangular bandpass filter depicted in (b). (d) The reconstructed phase calculated from the inverse Fourier transformation of the filtered signal of (b).

and inverse Fourier transformation, we obtain the complex signal I_{SSB},

$$I_{SSB}(z) = 0.5 I_0 C(z) e^{-i\left(\frac{2\pi(z-z_0)}{\Delta s P} + \phi_0\right)}, \tag{4}$$

from which the contrast curve $C(z)$ and the phase information $\phi_0(z)$ can be easily decoded.

A. Lower Limit of the Number of Sampling Steps

Beside getting rid of the stop-and-go problem, the novel sampling scheme with flying phase shifting offers one more significant improvement: the number E of sampling steps can be reduced, compared to classical phase-shifting SIM. In the following, we explain how to achieve the theoretical lower limit of sampling steps (exposures).

As noted earlier, we have the freedom to choose the sampling distance Δs and the number P of phase shifts per period. So we can adapt the carrier frequency within the contrast curve. (We emphasize that the width of the contrast curve is determined just by the aperture and fringe frequency.) What is the maximum sampling distance, i.e., the minimum number of exposures, to scan the contrast curve?

Referring to Fig. 3, the minimal allowed cut-off frequency ν_{cutoff} and the optimal carrier frequency $1/(\Delta s P)$ can be determined by satisfying the following two conditions: (1) both sidebands are located at the carrier frequency $1/(\Delta s P)$ of the modulated intensity signal [Fig. 3(a)] at half the cut-off frequency ν_{cutoff}; and (2) the full width $2(1/\text{FWHM}_C)$ of the side band, which is calculated from the half-width FWHM_C of envelope of the intensity (~ contrast curve), should be equal to the cut-off frequency ν_{cutoff}. With these rules we get

$$\frac{1}{\Delta s P} = 0.5\nu_{\text{cutoff}} \quad \text{and} \quad 2\frac{1}{\text{FWHM}_C} = \nu_{\text{cutoff}}. \tag{5}$$

With $\nu_{\text{cutoff}} = 0.5/\Delta s$, we obtain a remarkable result:

$$P = 4 \quad \text{and} \quad \frac{\text{FWHM}_C}{\Delta s} = 4. \tag{6}$$

The maximum sampling distance Δs is $\frac{1}{4}\text{FWHM}_C$. The minimal number of sampling points to be acquired within the FWHM_C of the contrast curve is 5 (including the left and right edges). This condition is achieved with four phase shifts per period ($P = 4$). The standard method requires at least three phase shifts at three positions of the contrast curve, or nine exposures. Our method is thus significantly more efficient. We note that the sampling distance Δs in Fig. 3(a) is smaller than $\text{FWHM}_c/4$, and the measurement is thus not as efficient as in the optimal case.

It may be helpful to explain the result above by considering the number of unknowns. As the mean intensity I_0 and phase ϕ_0 of a fixed sinusoidal pattern during depth scanning remain principally constant, after the first measurement at the first position, we need to measure only the contrast at the remaining two sampling positions, implying only five unknowns rather than nine unknowns.

We conclude that the AM-modulation/demodulation depth scan achieves the ultimate efficiency and solves the stop-and-go problem at the same time.

5. STRUCTURED-ILLUMINATION MACROSCOPY (SIMA) WITHOUT DEPTH SCAN

The logistics and speed requirements in industrial mass production call for a repeated cycle, where new samples are continuously fed into one side of the inspection station and taken out at the other side. An architecture that incorporates a vertical area scanning mechanism introduces discontinuity, disturbs the horizontal transportation of the samples, and wastes time for mechanical acceleration, deceleration, and stabilization. Vendors of inspection machines prefer a continuous process with just lateral sample movement, which is often implemented via line cameras.

One more argument against explicit longitudinal scanning (as in WLI and CM) is that the implementation demands highly complex mechanical components like vibrating tuning forks or oscillating reference mirrors. We will demonstrate that SIM can be implemented without any explicit longitudinal scan. The longitudinal scan can be integrated in a continuous (only) lateral scan. In [22,23,24], several methods for avoiding depth scanning are reported for WLI, CM, and passive focus variation. To our knowledge, there is still no solution like this for SIM. The method is a modification of the concept in section 4 and sketched in Fig. 4.

The basic idea is to perform just a lateral scan, and get the longitudinal scan as a present, without any explicit longitudinal motion. Only a continuous lateral scan is necessary. This makes SIM quite suitable for an industrial architecture, with the potential for ultra-fast operation.

As illustrated in Fig. 4, a static (no electronic pattern generator necessary!) sinusoidal fringe pattern is projected onto the object. In Fig. 4, the object is exemplified by a bar at a planar background. The sensor (and its focal plane) is tilted by a fixed angle θ to ensure that all points in the object volume are sampled by the image detector while the entire sensor is continuously moved along the x-axis, parallel to the sample surface. During the lateral scan, the camera takes exposures at constant time intervals. The time interval is adjusted in a way that individual object points are sequentially illuminated and observed with phase 0, $1/2\pi$, π, $3/2\pi$…, if four-phase shifting is applied. The intensity signals of a fixed object point at different depth steps are sampled by different points of the focus plane at different times. After complete data acquisition, the acquired images have to be virtually pipelined backward to generate an appropriate intensity stack. The intensity signal stored in all voxels at each lateral position corresponds to a modulated signal $I(z)$ as sampled by conventionally scanning described in section 4. The local contrast curve $C(z)$ is encoded in the envelope as depicted in Fig. 4. The height data are calculated, following the algorithm introduced before. The method with its continuous lateral scan avoids any explicit depth scan. The phase-shifting mechanism is automatically implemented during the lateral scan via electrical control of the exposure timing. There is no need for any additional mechanics, and a static pattern realized, for example, by chrome-on-glass is sufficient. This makes the "lateral scanning SIMA" very cost efficient.

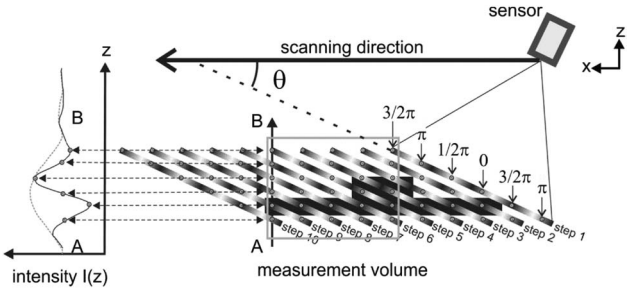

Fig. 4. Scheme of lateral scanning SIMA using four-phase shifting. The focus plane of the sensor (illustrated by the first sinusoidal bar at the right side) is tilted by an angle θ relative to the x-axis, which describes the scanning direction. While the sensor is moved along the x-direction, the focus plane moves along this direction as well, illustrated by the set of sinusoidal bars.

A serious technological limitation should be mentioned: the maximally allowed depth range Δz_o is limited by the necessary tilt angle θ. This angle is given by $\tan\theta = \Delta z_o/\Delta x$, where Δx is the field width. With a realistic limit $\theta_{\max} < 30°$, a large depth range will require a large field sensor. Another unfavorable aspect of this concept, when implemented with a tilted sensor, is that the tilted optical system can cause occlusion problems, which prevent symmetric angular dynamics. Nevertheless, this problem can be overcome by appropriate optical design, e.g., by exploiting the Scheimpflug condition.

To verify our method, we measured a wafer using a $20\times/0.5$ microscope objective with a field of view (FOV) of 320 µm × 240 µm. The sensor was tilted by $\theta \sim 15°$. By lateral scanning, we achieved a total FOV of 1.6 mm × 240 µm. (Additional results with a macroscopic field are shown in [25].) The raw intensity stack along one line in the z-direction is displayed in Fig. 5(a). The modulated intensity signal $I(z)$ along the black line in Fig. 5(a) is shown in Fig. 5(b). The complete height map in Fig. 6 demonstrates that the measurement with pure lateral scanning is possible. Although the measurement in the lab is still slow, a high-speed implementation is in principle only limited by the camera speed and by the available light intensity. The lateral resolution and the precision are limited by the same parameters as with standard SIM.

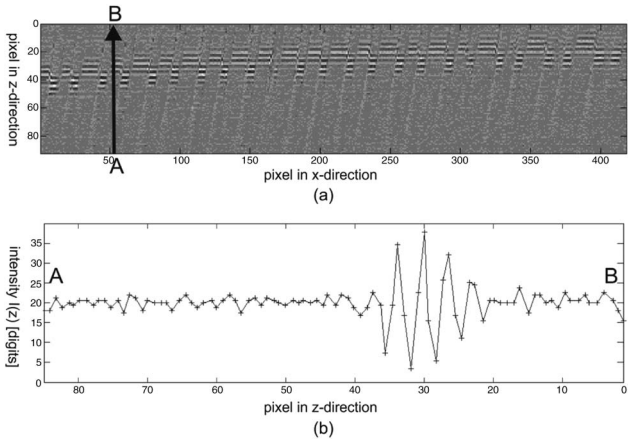

Fig. 5. (a) A cross section through the intensity data stack after post-processing (back-pipelined) raw images. (b) A raw intensity signal $I(z)$ in the z-direction at one pixel.

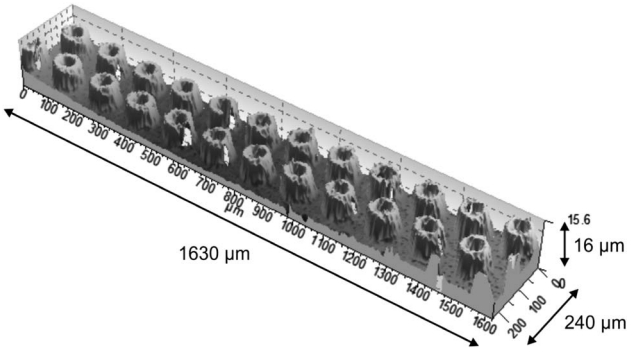

Fig. 6. A wafer measured with the lateral scanning structured illumination macroscopy. The size of the height map is extended to 1600 µm × 240 µm, whereas the FOV of the 20 × /0.5 microscope objective is only 320 µm × 240 µm.

We come back to our paradigm example: by exploiting our concept, the speed and field can be easily scaled up. Due to the improved information efficiency, only 50 depth scanning steps are necessary, instead of the 92 that are necessary with the conventional scanning strategy. With a fast camera ($S^{2D} = 500$ Mpix/sec,) the achievable space-bandwidth-speed product will be $S^{3D} = 10\ ^{3D}$Mpix/sec, which is two to 10 times larger than commercially available SIM and CM systems. The area speeds $S^{A} = 40$ cm^2/sec($\delta x \delta y = 25$ µm^2) and $S^{3D} = 160\ ^{3D}$Mpix/sec required in Table 1 cannot yet be achieved with one sensor. However, due to its highly cost-effective hardware implementation, a parallel use of ∼16 lateral scanning SIMA systems appears to be realistic. So our lateral scanning strategy might fulfill the target speed specification of high-speed bump inspection with low technological expense.

6. SUMMARY AND CONCLUSION

In this paper, we discuss the "speed" of 3D sensors, first in a general way to understand why 3D sensors are slow compared to 2D data sensors. The principal reason is the large number E of necessary exposures essentially caused by depth scanning and phase shifting. A higher speed can easily be achieved by carefully reducing requirements such as the lateral resolution and measuring range. Rules are given to do this in an optimal way.

Even with an optimized number of exposures, depth scanning wastes much time if it is performed in a stop-and-go mode. We demonstrate that stop-and-go can be avoided by applying what we call "flying phase shifting," where phase shifting is performed simultaneously with depth scanning. The decoding of the modified contrast function is done by single-sideband demodulation. The method even significantly reduces the number of scanning steps compared to the standard method.

Via an extension of this concept, the depth scan can be completely avoided. Just a continuous transverse (x-) scan is necessary. The achievable area speed is now only limited by the camera speed. The hardware is simple, and the technical implementation is simple and cost efficient. These conditions allow a further increase in speed by the parallelization of several sensors. These remarkable features of lateral scanning SIMA make it a candidate for high-speed 3D quality control in a factory.

Funding. Deutsche Forschungsgemeinschaft (DFG)Az Ha 1319/13-1.

Acknowledgment. We thank the Deutsche Forschungsgemeinschaft (Az Ha 1319/13-1) for funding this research, and Markus Vogel as well as William T. Rhodes for fruitful discussions. We note that Alexander Kessel is responsible for the idea of the "flying phase shift" for SIM.

REFERENCES

1. Z. Yang, A. Kessel, and G. Häusler, "Better 3D inspection with structured illumination: signal formation and precision," Appl. Opt. **54**, 6652–6660 (2015).
2. R. G. Dorsch, G. Häusler, and J. M. Herrmann, "Laser triangulation: fundamental uncertainty in distance measurement," Appl. Opt. **33**, 1306–1314 (1994).
3. C. Wagner and G. Häusler, "Information theoretical optimization for optical range sensors," Appl. Opt. **42**, 5418–5426 (2003).
4. G. Häusler, C. Faber, F. Willomitzer, and P. Dienstbier, "Why can't we purchase a perfect single shot 3D-sensor?," Proc. DGaO A8 (2012).
5. G. Häusler and D. Ritter, "Parallel three-dimensional sensing by color-coded triangulation," Appl. Opt. **32**, 7164–7169 (1993).
6. J. Tajima and M. Iwakawa, "3D Data acquisition by rainbow range finder," in *Proceedings of 10th International Conference on Pattern Recognition* (IEEE, 1990), Vol. **1**, pp. 309–313.
7. R. Lange, P. Seitz, A. Biber, and S. Lauxtermann, "Demodulation pixels in CCD and CMOS technologies for Time-of-Flight ranging," Proc. SPIE **3965**, 3965A (2000).
8. P. M. Griffin, L. S. Narasimhan, and S. R. Yee, "Generation of uniquely encoded light patterns for range data acquisition," Pattern Recogn. **25**, 609–616 (1992).
9. L. Zhang, B. Curless, and S. M. Seitz, "Rapid shape acquisition using color structured light and multi-pass dynamic programming," presented at Proc. of the 1st International Symposium on 3D Data Processing, Visualization and Transmission (3DPVT), Padova, Italy (2002).
10. V. Srinivasan, H. C. Liu, and M. Halioua, "Automated phase-measuring profilometry of 3-D diffuse objects," Appl. Opt. **23**, 3105–3108 (1984).
11. T. Dresel, G. Häusler, and H. Venzke, "3D-sensing of rough surfaces by 'coherence radar'," Appl. Opt. **31**, 919–925 (1992).
12. O. Hýbl and G. Häusler, "Information efficient whit e-light interferometry," presented at Proc. ASPE 2010 Summer Topical Meeting, Asheville, North Carolina (ASPE, 2010).
13. R. Artigas, F. Laguarta, and C. Cadevall, "Dual-technology optical sensor head for 3D surface shape measurements on the micro and nano-scales," Proc. SPIE **5457**, 166–174 (2004).
14. M. Schwertner, "Verfahren und Anordnung zur optischen Abbildung mit Tiefendiskriminierung," German patent DE 102007018048 (October 16, 2008).
15. J. J. Xu, "3-D optical microscope," US patent US 7729049 (June 1, 2010).
16. M. Vogel, Z. Yang, A. Kessel, C. Kranitzky, C. Faber, and G. Häusler, "Structured-illumination microscopy on technical surfaces: 3D metrology with nanometer sensitivity," Proc. SPIE **8082**, 80820S (2011).
17. A. Bielke, A. Kessel, M. Vogel, Z. Yang, C. Faber, and G. Häusler, "Fast acquisition of 3D-data with structured illumination microscopy," Proc. DGaO, P036 (2011).
18. K. Jörner and R. Windecker, "Absolute macroscopic 3-D measurement with the innovative depth-scanning fringe projection technique (DSFP)," Optik **112**, 433–441 (2001).
19. G. S. Kino and S. S. C. Chim, "Mirau correlation microscope," Appl. Opt. **29**, 3775–3783 (1990).

20. S. S. C. Chim and G. S. Kino, "Three-dimensional image realization in interference microscopy," Appl. Opt. **31**, 2550–2553 (1992).
21. Q. Kemao, H. Wang, and W. Gao, "Windowed Fourier transform for fringe pattern analysis: theoretical analyses," Appl. Opt. **47**, 5408–5419 (2008).
22. D. M. Ljubicic and B. W. Anthony, "High speed 3D profilometer for measurement of transparent parts," Proc. SPIE **8082**, 808211 (2011).
23. Y. Y. Lan, J. L. Chen, W. C. Wang, and L. R. Chang, "Large-scale 3-D profilometer," Proc. SPIE **7073**, 70732J (2008).
24. A. Olszak, "Lateral scanning white-light interferometer," Appl. Opt. **39**, 3906–3913 (2000).
25. Z. Yang and G. Häusler, "Lateral scanning 'Structured-Illumination-MAcroscopy' for high speed electronic inspection," Proc. DGaO, A8 (2014).